Emiss. Control Sci. Technol. (2016) 2:57–65
DOI 10.1007/s40825-016-0037-z

TWC Performance of Honeycomb Catalysts Coated with Pd-Supported $10Al_2O_3 \cdot 2B_2O_3$ and Its Cation-Substituted Compounds

Yuki Nagao[1,2] · **Yunosuke Nakahara**[1] · **Takahiro Sato**[1] · **Shuji Nakano**[2] · **Masato Machida**[2,3]

Received: 18 November 2015 / Revised: 5 March 2016 / Accepted: 11 March 2016 / Published online: 21 April 2016

Abstract TWC performances of honeycomb-coated Pd catalysts supported on $10Al_2O_3 \cdot 2B_2O_3$ ($Al_{20}B_4O_{36}$, 10A2B) and its Fe-substituted analogue ($FeAl_{19}B_4O_{36}$, Fe-10A2B) were studied using simulated exhaust gas mixtures. A monolayer-coated honeycomb containing Pd/10A2B was able to achieve higher conversion of CO, C_3H_6 and NO in stoichiometric gas mixtures after the light-off temperature compared to a honeycomb containing Pd/γ-Al_2O_3. Bilayer-coated honeycombs comprising a top Rh layer (Rh/CeO_2-ZrO_2) and a bottom Pd layer (Pd/10A2B or Pd/γ-Al_2O_3) with varying Rh:Pd ratios were evaluated under stoichiometric conditions. The Rh loading in the top layer could be decreased while preserving higher levels of conversion at 400 °C when Pd/10A2B was used as opposed to Pd/γ-Al_2O_3. Another monolayer-coated honeycomb comprising Pd/Fe-10A2B demonstrated higher NO conversion under fuel-rich conditions compared to conventional Pd catalysts that were loaded on 10A2B, γ-Al_2O_3 and Pd/CeO_2-ZrO_2. Pd/Fe-10A2B promoted the conversion of NO to NH_3 because CO–H_2O and subsequent NO–H_2 reactions were accelerated.

Keywords Three-way catalyst · Pd catalyst · $10Al_2O_3 \cdot 2B_2O_3$ · Honeycomb

1 Introduction

The three-way catalysis (TWC) system is the current exhaust purification technology used for gasoline-fueled automobiles, which requires platinum group metals (PGMs) such as Pt, Pd and Rh as active catalyst components [1–5]. As automobile usage in emerging countries is rapidly increasing, automotive emission regulations are more severely restricted. As such, the demand for PGMs is increasing and thus the development of catalysts using lower amounts of PGMs is required. The catalyst design strategy for this purpose is based on various metal oxide support interactions [6–17]. Thus, further development of novel support materials that can stabilise active PGM elements is challenging.

Among PGM elements, palladium (Pd) has high catalytic activities especially for oxidation reactions in TWC. The Pd catalyst deactivation during thermal ageing is caused by the sintering of metallic Pd, which is especially pronounced under fuel-rich conditions compared to lean environment [18, 19]. Although γ-Al_2O_3 has been widely used as support for Pd catalysts, we are interested in the use of aluminium oxide borate ($10Al_2O_3 \cdot 2B_2O_3$, 10A2B). The first catalytic application of 10A2B was reported by Garbowski et al., who studied characteristics as a support for high-temperature methane combustion [20]. More recently, we reported that 10A2B is a potential support material suitable for Pd, having a higher specific surface area and thermal stability than conventional

Electronic supplementary material The online version of this article (doi:10.1007/s40825-016-0037-z) contains supplementary material, which is available to authorized users.

✉ Yuki Nagao
y_nagao@mitsui-kinzoku.co.jp

✉ Masato Machida
machida@kumamoto-u.ac.jp

[1] Catalysts Division, Engineered Materials Sector, Mitsui Mining & Smelting Co., Ltd., 1013-1 Ageoshimo, Ageo, Saitama 362-0025, Japan

[2] Department of Applied Chemistry and Biochemistry, Graduate School of Science and Technology, Kumamoto University, 2-39-1 Kurokami, Chuo, Kumamoto 860-8555, Japan

[3] Unit of Elements Strategy Initiative for Catalysts & Batteries, Kyoto University, 1-30 Goryo-Ohara, Nishikyo, Kyoto 615-8245, Japan

γ-Al_2O_3 [21, 22]. The most beneficial feature of 10A2B is its stability under high-temperature water vapour, which is an important property for TWC support materials. Another interesting feature is its cation-substitution capability; among various transition metal cations, Fe^{3+} is most easily accommodated in the 10A2B structure. This structural modification significantly enhanced the NO reduction efficiency under fuel-rich conditions with an air-to-fuel ratio (A/F) of <14.6 [22]. Moreover, the redox reaction between Fe^{3+} and Fe^{2+} can contribute to the oxygen storage capacity (OSC) of the catalyst [22]. According to the fundamental results of 10A2B powders, we have extended our research to honeycomb-shaped catalysts for practical applications in the TWC system. In this study, we have prepared two types of monolithic honeycomb catalysts using 10A2B and Fe-10A2B as Pd supports. The TWC performance of Rh/Pd bilayer-coated honeycomb catalysts in simulated exhaust comprising NO–CO–C_3H_6–O_2–CO_2–H_2O gas mixtures was evaluated as a function of the Rh:Pd loading ratio. Furthermore, the Pd/Fe-10A2B monolayer catalyst was studied under rich conditions (A/F < 14.6) to induce higher NO conversion compared to a reference catalyst (Pd/CeO_2-ZrO_2).

2 Experimental

2.1 Catalyst Preparation

The powders of 10A2B and Fe-10A2B were prepared via a wet process. H_3BO_3 (Wako Pure Chemicals) was dissolved in water and boehmite (Disperal, Sasol) was added with a molar ratio of Al:B = 20:4.8 under vigorous stirring. A 20 % excess of H_3BO_3 was used as it is volatilised during subsequent drying and calcination processes. The as-obtained slurry was dried at 120 °C for 12 h, ground and heated at 300 °C for 1 h. Finally, the as-obtained powder was calcined at 1000 °C for 5 h in air to complete solid-state reactions to a 10A2B phase. γ-Al_2O_3 was prepared from boehmite as a reference by drying and calcination at 600 °C. Lanthanum (3 mol%) was impregnated in 10A2B and γ-Al_2O_3 using an aqueous solution of $La(NO_3)_3$ (Wako Pure Chemicals), followed by drying and calcining at 600 °C for 3 h in air. The La addition is known to stabilise γ-Al_2O_3 against phase transformation to α-Al_2O_3 [23–25]. Fe-10A2B was prepared in a manner similar to 10A2B by using H_3BO_3, $Fe(NO_3)_3$ (Wako Pure Chemicals) and boehmite. Solid solutions of CeO_2-ZrO_2 of 1:9 and 4:6 M ratios were prepared as reference supports via co-precipitation method. To aqueous solutions containing $Ce(NO_3)_3$ and $ZrO(NO_3)_2$ (Wako Pure Chemicals), a 12 % NH_3 solution was added under vigorous stirring until the pH reached 10. The precipitates were washed with water, dried and calcined at 700 °C for 3 h to form single-phase solid solutions of tetragonal fluorite-type structure (see Fig. S1 in Electronic supplementary material (ESM)). As-prepared compounds with CeO_2:ZrO_2 M ratios of 1:9 and 4:6 were used for the top and bottom layers, respectively, of bilayer-coated honeycomb catalysts.

As shown in Fig. 1, three types of honeycomb-coated catalysts were prepared in the present study. For preparing honeycomb catalysts, various slurries were prepared by ball-milling the catalyst powders, inorganic binders and water. Monolayer-coated honeycombs (type A) were prepared by dipping a cordierite honeycomb (25.4 mmφ × 30 mm, 600 cells in^{-2}, NGK Insulator) into the slurry containing either 10A2B or γ-Al_2O_3, which was followed by impregnation with an aqueous solution of $Pd(NO_3)_2$ (Tanaka Kikinzoku), drying and calcining at 600 °C for 3 h in air. The Pd loading of the as-calcined honeycomb catalysts corresponded to 1.3 g L^{-1}. Bilayer-coated honeycombs (type B) were prepared by a stepwise dipping process. First, the cordierite honeycomb was dipped into the slurry containing either 10A2B or γ-Al_2O_3 and CeO_2-ZrO_2 (CeO_2:ZrO_2 = 4:6) and was subsequently impregnated with an aqueous solution of $Pd(NO_3)_2$. The mass ratio of 10A2B or γ-Al_2O_3 and CeO_2-ZrO_2 was 1:1. After calcining at 600 °C for 3 h in air, a second dipping was conducted using a slurry containing CeO_2-ZrO_2 (CeO_2:ZrO_2 = 1:9) and γ-Al_2O_3. The mass ratio of CeO_2-ZrO_2 and γ-Al_2O_3 was 3:1. This was followed by impregnation with an aqueous solution of $Rh(NO_3)_3$ (Tanaka Kikinzoku), drying and calcining at 600 °C for 3 h in air. As-calcined bilayer-coated honeycomb catalysts with a top Rh layer and a bottom Pd layer contained 1.0 g L^{-1} of Rh + Pd with different weight ratios of Pd:Rh (3:1, 5:1, 10:1 and 19:1). Different monolayer-coated honeycombs (type C) were prepared in a similar manner using the same cordierite honeycombs and a slurry containing either 10A2B, γ-Al_2O_3, CeO_2-ZrO_2 (CeO_2:ZrO_2 = 4:6) or Fe-10A2B. After subsequent impregnation with an aqueous solution of $Pd(NO_3)_2$ and drying,

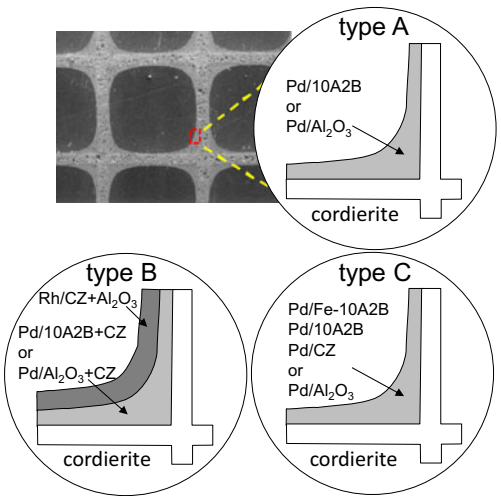

Fig. 1 Schematic illustrations of three types of honeycomb catalysts. CZ means CeO_2–ZrO_2

they were calcined at 600 °C for 3 h in air. The Pd loading of as-calcined honeycomb catalysts corresponded to 0.7 g L^{-1}.

2.2 Catalyst Characterisation

X-ray diffraction (XRD) patterns of 10A2B and Fe-10A2B powders were obtained using a Rigaku RINT-TTR III diffractometer with Cu Kα radiation (50 kV, 30 mA). The metal loading was analysed by the ICP analysis, which agreed with the calculated values based on the synthesis procedure described above within an error of 10 %. Brunauer–Emmett–Teller (BET) surface areas (S_{BET}) were calculated using N_2 adsorption isotherms obtained at −196 °C (Belsorp-mini, Bel Japan). The Pd metal dispersion was evaluated using pulsed CO chemisorption at 50 °C (Belcat, Bel Japan) after sample reduction with H_2 at 400 °C. The metal dispersion is expressed as the molar ratio of chemisorbed CO per loaded Pd (CO/Pd). The microstructure of the materials was observed using a field emission scanning electron microscope (XL30, FEI) and a scanning electron microscope (SEM : Miniscope TM3000, Hitachi). The spatial distribution of Rh and Pd in bilayer-coated honeycombs was analysed by X-ray line analysis technique (Shimadzu EPMA-1720H).

2.3 Catalyst Performance Testing

Prior to the catalytic tests, all as-prepared honeycomb catalysts were thermally aged at 1000 °C for 25 h by continuously switching between two gas feeds, i.e. stoichiometric (50 s) and lean conditions (50 s). The stoichiometric gas composition (A/F = 14.6) was C_3H_6 (1670 ppm), O_2 (0.75 %) and N_2 (balance), while the lean gas was composed of air with 10 % H_2O. Catalytic activity tests on the honeycomb catalysts were performed in a flow reactor at atmospheric pressure. Catalytic light-off tests of the stoichiometric simulated gas stream of CO (0.73 %), C_3H_6 (400 ppm), NO (500 ppm), O_2 (0.50 %), CO_2 (14 %), H_2O (10 %) and N_2 (balance) over the honeycomb catalysts (types A and B) were performed at a heating rate of 20 °C min^{-1} and space velocity (SV) of 98,000 h^{-1}. The gas composition corresponded to the stoichiometric A/F of 14.6. The concentrations of CO, C_3H_6 and NO in the effluent gas were analysed online using a motor exhaust gas analysis system (MEXA 9100, Horiba) equipped with non-dispersive infrared detectors and a flame ionisation detector.

The steady-state catalyst performance for honeycomb catalysts (type C) was evaluated at 400 °C using gas mixtures containing CO, C_3H_6, H_2, NO, O_2, CO_2, H_2O and N_2 balance with various A/F values (14.2–14.8) at SV = 98,000 h^{-1} (See Table S1 in ESM). The concentrations of CO, C_3H_6 and NO in the effluent gas were analysed online using an exhaust gas analyser (MEXA 9100). Catalytic light-off tests on the honeycomb catalysts (type C) were performed in three different modes (I, II and III) under rich conditions (A/F = 14.2). Mode I used gas mixtures containing NO, CO, C_3H_6, H_2, O_2, H_2O and N_2 balance, whereas modes II and III excluded C_3H_6 and C_3H_6/H_2, respectively (See Table S2 in ESM). The effluent gas composition was analysed online using an exhaust gas analyser (Best Sokki, Sesam3-N and Bex-5200C) equipped with an FT-IR spectrometer and a flame ionisation detector.

3 Results and Discussion

3.1 Type A Monolayer Catalysts

Figure 2 shows SEM images of γ-Al_2O_3 and 10A2B after calcination at 1000 °C. Contrary to the amorphous texture of γ-Al_2O_3, 10A2B was composed of larger particles (~50–150 nm) with an elliptical shape. The S_{BET} value of 10A2B (70 m^2 g^{-1}) was less than that of γ-Al_2O_3 (81 m^2 g^{-1}), whereas the Pd metal dispersions for their Pd-supported catalysts were nearly identical (CO/Pd values close to 50 %). Table 1 shows the influence of thermal ageing under dry and

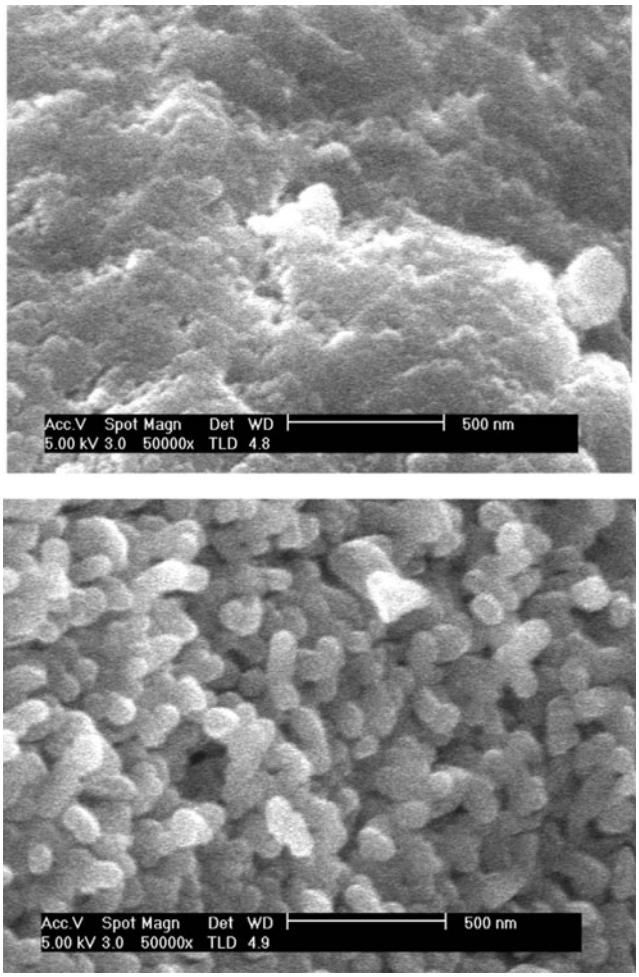

Fig. 2 SEM images of γ-Al_2O_3 (*top*) and 10A2B (*bottom*) after calcination at 1000 °C

Table 1 BET surface area (S_{BET}/ $m^2\ g^{-1}$) of support materials after thermal ageing

Support	Dry air[b]				10 % H_2O/air[c]			
	900 °C	1000 °C	1100 °C	1200 °C	900 °C	1000 °C	1100 °C	1200 °C
10A2B[a]	70	70	22	10	59	43	18	4
γ-Al_2O_3[a]	81	68	54	6	68	50	7	1

[a] Calcined at 1000 °C before thermal ageing

[b] After thermal ageing for 10 h under dry air

[c] After thermal ageing for 25 h in 10 % H_2O/air

humidified atmospheres on the S_{BET} value of each support material. The S_{BET} value of 10A2B decreased with increasing temperature and was less than that of γ-Al_2O_3 when calcined under dry air. However, the result was different when the calcined sample was further heated under a stream of 10 % H_2O/air; 10A2B had a greater S_{BET} at 1200 °C, while γ-Al_2O_3 showed more steep sintering because the phase transformation to α-Al_2O_3 was significantly accelerated (see Fig. S2 in ESM). Similar effects of water vapour on the phase transformation of transition alumina are reported in the literature [26–28]. By contrast, water vapour had no detectable influence on the structure and the crystallinity of 10A2B (see Fig. S3 in ESM). Thus, stability under hydrothermal conditions is a beneficial feature of 10A2B as a support material for automotive catalysts.

The effect of the support material on TWC performance was studied using monolayer-coated honeycomb catalysts (type A). Figure 3 shows the catalytic light-off curves of the stoichiometric simulated gas mixture (A/F = 14.6) for honeycomb catalysts containing Pd/10A2B or Pd/γ-Al_2O_3. Both catalysts displayed very similar light-off curves for CO, C_3H_6 and NO. To compare their differences, Table 2 lists the light-off temperatures (T_{50}), which was defined as the temperature at which the conversion of each gas species reaches 50 %, as well as the apparent conversion at 400 °C (η_{400}), which was used to evaluate the performance after the light-off temperature. The T_{50} values for Pd/10A2B were 6–8 °C higher than that of Pd/γ-Al_2O_3 for each gas species. Nevertheless, the former achieved 3–4 % higher η_{400} values than the latter, with the values for CO and C_3H_6 being especially close to complete removal. One may point out that the differences of η_{400} values are too small to correlate with the catalytic activity. However, the difference in the η_{400} values between Pd/10A2B and Pd/Al_2O_3 is reproducible and is in accordance with the activity trend of bilayer-coated honeycomb catalysts as described in the following section. Because the η_{400} value is regarded as an activity measure after the light-off, which is a very important feature considering the stringent automotive emission regulations.

3.2 Type B Bilayer Catalysts

Figure 4 shows a SEM image of the fracture surface of an as-prepared bilayer honeycomb catalyst with a top Rh catalyst layer and a bottom Pd catalyst layer. The top layer is approximately 40-μm thick at the corner of the square cells and contains Rh loaded on CeO_2-ZrO_2 and γ-Al_2O_3, whereas the bottom layer is approximately 90-μm thick at the corner of the square cells and contains Pd loaded on 10A2B and CeO_2-ZrO_2. The spatial distribution of Rh and Pd in each layer was demonstrated by SEM/EDX analysis (Fig. S4 in ESM). These layers were in close contact with the surface of the cordierite honeycomb substrate. Similar microstructure was observed for another bilayer honeycomb catalyst

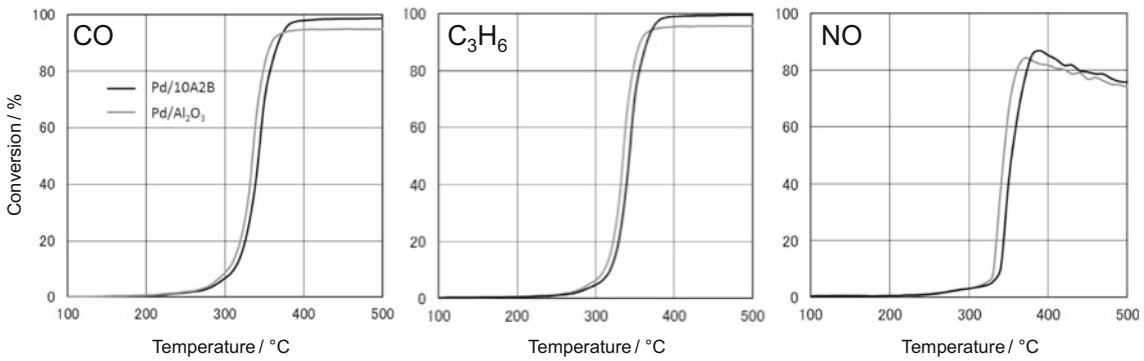

Fig. 3 Catalytic light-off curves of CO, C_3H_6 and NO over monolayer honeycomb catalysts (type A) under stoichiometric conditions (A/F = 14.6). Temperature ramp 20 °C min^{-1}

Table 2 Catalytic activities of Pd/10A2B and Pd/γ-Al_2O_3

Sample	T_{50}[a]/°C			η_{400}[b]/%		
	CO	C_3H_6	NO	CO	C_3H_6	NO
Pd/10A2B	344 ± 4	344 ± 2	352 ± 5	98.0 ± 0.2	99.0 ± 0.3	85.2 ± 1.9
Pd/γ-Al_2O_3	336 ± 3	336 ± 2	346 ± 5	94.7 ± 0.2	95.2 ± 0.2	81.7 ± 1.9

Errors were obtained in eight runs of the catalytic reaction tests

[a] Reaction temperature at which the conversion of each gas species reached 50 %

[b] Apparent conversion at 400 °C after the light-off of simulated gas mixtures

composed of a top Rh/CeO_2-ZrO_2/Al_2O_3 layer (CeO_2:ZrO_2 = 1:9) and a bottom Pd/Al_2O_3/CeO_2-ZrO_2 layer (CeO_2:ZrO_2 = 4:6). Therefore, the only difference between these two bilayer honeycomb catalysts is their support materials (10A2B or Al_2O_3) in the bottom layer as shown in Fig. 1.

These two types of bilayer honeycomb catalysts (type B) with different Rh:Pd ratios were used to simulate a TWC reaction. The total loading of Rh + Pd (1.0 g L^{-1}) was maintained unchanged. Figure 5 shows the catalytic light-off curves for the stoichiometric simulated gas mixture (A/F = 14.6). The light-off temperature (T_{50}) was found to be dependent on the support materials for the bottom Pd layer; catalysts containing Pd/10A2B were inferior to Pd/γ-Al_2O_3.

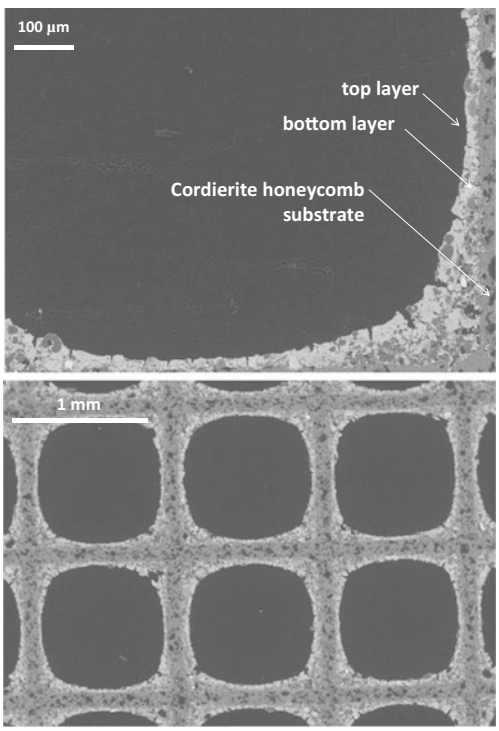

Fig. 4 SEM image of the fracture surface of the bilayer-coated honeycomb catalyst (type B) with a Pd/10A2B + CeO_2-ZrO_2 bottom layer and Rh/CeO_2 − ZrO_2 + γ-Al_2O_3 top layer

Conversely, catalysts containing Pd/10A2B demonstrated higher conversion efficiencies after the light-off (η_{400}). These trends are in accordance with those of the aforementioned monolayer honeycomb catalysts (type A, Fig. 3). To elucidate the effect of Rh:Pd ratios on the catalytic performance, these two activity measurements (T_{50} and η_{400}) were plotted as a function of the Rh:Pd ratio, as shown in Fig. 6. To confirm the reproducibility of the plots in Fig. 6, the light-off reaction test was performed eight times using several batches of honeycombs prepared using the same procedure. The observed relative errors for T_{50} values in Fig. 6a were 2.1 %(CO), 1.2 %(HC) and 2.9 %(NO_x), and those for η_{400} values in Fig. 6b were 0.4 %(CO), 0.5 %(HC) and 4.1 %(NO_x). At the highest Rh content (Pd:Rh = 3:1, Rh = 0.25 g L^{-1}), the catalyst with 10A2B showed higher T_{50} values than that with γ-Al_2O_3. However, the difference in T_{50} was not obvious when the Rh content was less than 0.2 g L^{-1}. As the Rh loading was decreased, η_{400} continuously decreased for the honeycomb comprising a Pd/γ-Al_2O_3 bottom layer. In contrast, the η_{400} value was maintained almost unchanged (>96 % conversion) when Pd/10A2B was used rather than Pd/γ-Al_2O_3 as the bottom catalyst layer. It was suggested that the Pd catalyst on the bottom layer showed higher catalytic performance after the light-off temperatures (≥400 °C) regardless of the amount of Rh. This is consistent with the results shown in Fig. 3 because when the Pd-only catalyst (type A) was loaded on 10A2B, higher conversions were achieved after the light-off temperature compared with Pd/γ-Al_2O_3. Although Rh is an indispensable active component of the TWC system, particularly for efficient conversion of NO to N_2 [2, 29, 30], it is one of the rarest platinum group metals for this purpose. The present results on bilayer honeycomb catalysts demonstrated that the Rh content can be decreased without destroying the catalytic performance by using Pd/10A2B.

3.3 Type C Monolayer Catalysts

The effect of Fe-substitution in 10A2B on the catalytic performance was studied using monolayer-coated honeycombs (type C). Substitution of Fe for the Al site in 10A2B was demonstrated using XRD (See Fig. S5 in ESM). Although Fe-substitution did not affect the particle morphology, the S_{BET} value of Fe-10A2B (44 m^2 g^{-1}) was smaller than that of neat 10A2B (70 m^2 g^{-1}). Figure 7 shows the A/F dependence on conversion of CO, C_3H_6 and NO at 400 °C. In the lean region (A/F > 14.6), CO and C_3H_6 were completely converted to CO_2/H_2O with all catalysts, while NO conversion was strongly inhibited because of excess O_2 in the gas phase. In the rich region (A/F < 14.6), Pd/Fe-10A2B showed higher conversion of C_3H_6 and NO compared to Pd/γ-Al_2O_3 and Pd/10A2B. According to our previous study on powdered catalysts [22], Fe-substitution improves the catalytic NO

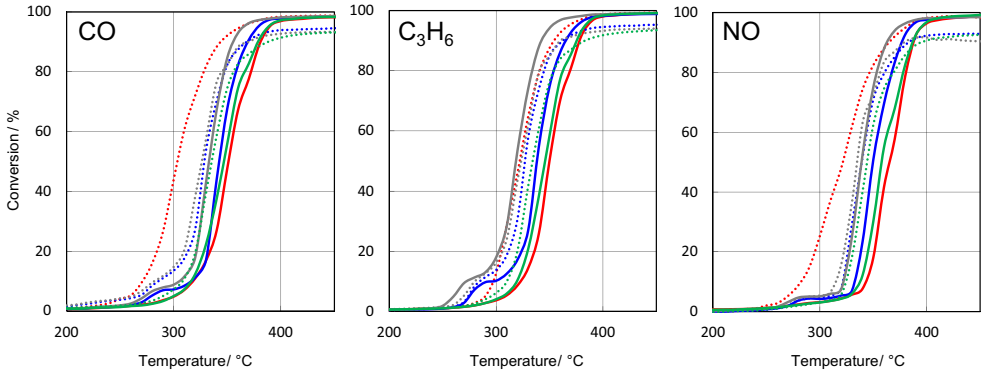

Fig. 5 Catalytic conversion of CO, C_3H_6 and NO over bilayer-coated honeycomb catalysts (type B) under stoichiometric conditions (A/F = 14.6, 20 °C min^{-1})

	Rh / g L^{-1}	Pd / g L^{-1}	Support in bottom layer
	0.25	0.75	10A2B
	0.25	0.75	Al_2O_3
	0.17	0.83	10A2B
	0.17	0.83	Al_2O_3
	0.09	0.91	10A2B
	0.09	0.91	Al_2O_3
	0.05	0.95	10A2B
	0.05	0.95	Al_2O_3

conversion in the rich region (A/F < 14.6) because of enhanced activity for NO–C_3H_6, CO–H_2O and NO–H_2 reactions. Since the higher conversion of C_3H_6 and NO was also observed for Pd/CeO_2-ZrO_2, the following studies were performed using Pd/CeO_2-ZrO_2 as a reference catalyst. Our previous study also demonstrated that the redox reaction between Fe^{3+} and Fe^{2+} in Fe-10A2B generates an OSC that causes an efficient buffering effect on dynamic A/F fluctuation, which is a well-known function of CeO_2-ZrO_2 [31–35]. However, its contribution to the present catalytic performance under a static rich condition should be negligible.

Figure 8 shows the catalytic light-off curves for CO, C_3H_6 and NO in the CO–C_3H_6–H_2–NO–O_2–H_2O reaction (mode I, A/F = 14.2, see Table S2 in EMS for detailed gas compositions) over monolayer honeycomb catalysts (type C) comprising Pd/CeO_2-ZrO_2 and Pd/Fe-10A2B. Evidently, higher conversion of NO occurred with Pd/Fe-10A2B compared to Pd/CeO_2-ZrO_2, although their conversions of C_3H_6 and CO were comparable. On NO reduction, N_2O was negligible while nearly stoichiometric NH_3 was yielded over both catalysts. Note that NO conversion to NH_3 began at ~200 °C and conversion of CO and C_3H_6 were negligible at this temperature, suggesting the occurrence of an NO–H_2 reaction. However, the NO conversion levelled off and then decreased at ≥300 °C. The irregular shape of NO conversion is possibly associated with the increased rate of the H_2–O_2 reaction at this temperature. However, further increase in temperature led to an increase in the NO–H_2 reaction because CO–H_2O and C_3H_6–H_2O reactions began to produce H_2.

To demonstrate this hypothesis, catalytic light-off tests of CO and NO in the CO–NO–H_2–O_2–H_2O reaction (mode II) were performed at A/F = 14.2 (Fig. 9). Upon

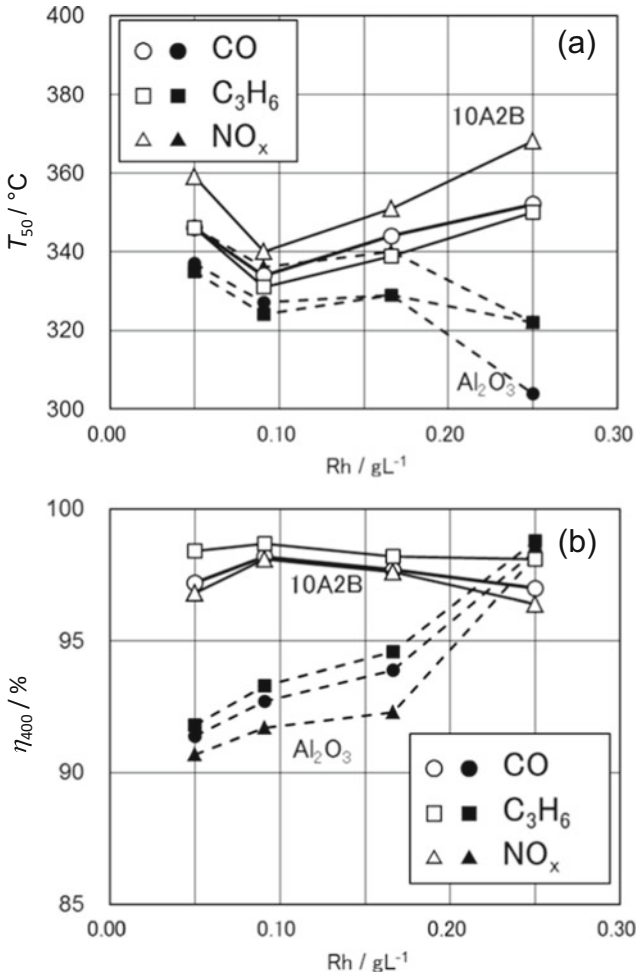

Fig. 6 **a** Light-off temperature (T_{50}). **b** Conversion at 400 °C (η_{400}) as a function of Rh loading for Rh/Pd bilayer-coated honeycomb catalysts (type B) containing Pd/10A2B or Pd/γ-Al_2O_3 bottom layers. Total metal loading (Rh + Pd) is constant at 1.0 g L^{-1}

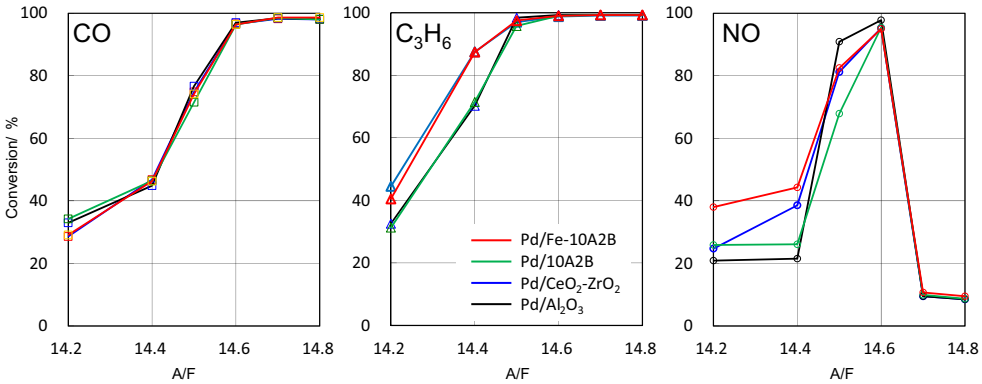

Fig. 7 Catalytic conversion of CO, C_3H_6 and NO at 400 °C over monolayer honeycomb catalysts (type C) in the range of $14.2 \leq A/F \leq 14.8$

removal of C_3H_6, NO reduction to NH_3 was further accelerated at lower temperatures (<200 °C) compared with Fig. 8. In addition, the irregular shape of both NO conversion and NH_3 concentration were no longer observed because of the higher H_2/O_2 ratio in the gas feed. Moreover, the suppression of CO–O_2 reaction is also beneficial for H_2 production via the water-gas shift reaction. Even under these conditions, Pd/Fe-10A2B was superior to Pd/CeO_2-ZrO_2 for the NO–H_2 reaction. Figure 10 shows the results of the CO–NO–O_2–H_2O reaction (mode III). Because H_2 was absent in this case, a higher light-off temperature was required for NO (≥240 °C) compared to Figs. 8 and 9. Thus, NO conversion was driven by the CO–H_2O reaction followed by the NO–H_2 reaction. In addition, the NO–CO reaction may contribute to this conversion, as can be assumed from the higher concentrations of N_2O compared to Figs. 8 and 9. Importantly, Pd/Fe-10A2B exhibited higher NO conversion than Pd/CeO_2-ZrO_2 over the entire temperature range. Under rich conditions, Pd/Fe-10A2B can contribute to NO conversion, which is superior to Pd/γ-Al_2O_3 and Pd/10A2B, because of its higher catalytic activity for the NO–H_2 reaction to NH_3.

4 Conclusions

Three different honeycomb-coated catalysts containing 10A2B and Fe-10A2B as supports for Pd were prepared and their catalytic performances under simulated TWC conditions were compared to those of conventional Pd/γ-Al_2O_3 and/or Pd/CeO_2-ZrO_2 catalysts. The monolayer-coated Pd/10A2B catalyst (type A) achieved higher conversion of CO, C_3H_6 and NO after the light-off temperature (400 °C), compared to conventional Pd/γ-Al_2O_3. The Rh/Pd bilayer-coated honeycomb catalysts (type B) using Pd/10A2B were also able to preserve higher levels of CO, HC and NO conversion at 400 °C compared with Pd/γ-Al_2O_3 when Rh loading in the top layer was decreased. These results imply that Pd/10A2B is

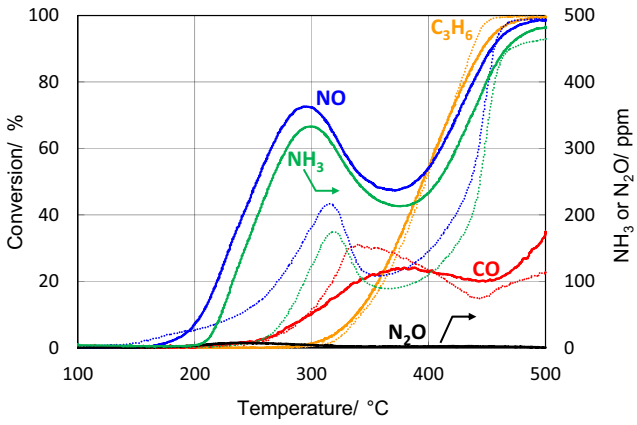

Fig. 8 Catalytic light-off curves of CO–C_3H_6–H_2–NO–O_2–H_2O–N_2 and NH_3/N_2O formation over monolayer honeycomb catalysts (type C, mode I) at A/F = 14. *Solid lines* Pd/Fe-10A2B. *Dotted lines* Pd/CeO_2-ZrO_2. Temperature ramp 20 °C min^{-1}

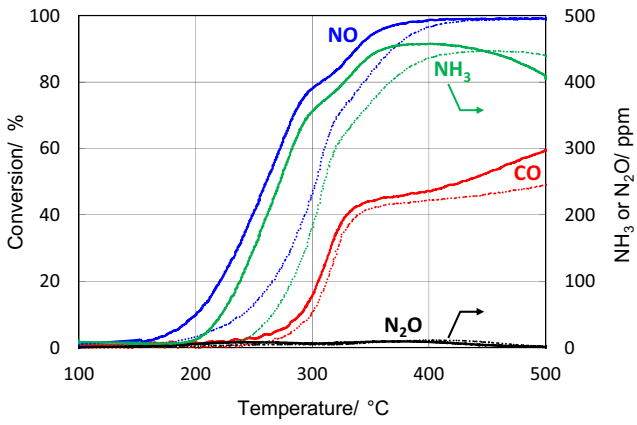

Fig. 9 Catalytic light-off curves of CO–NO–H_2–O_2–H_2O–N_2 and NH_3/N_2O formation over monolayer honeycomb catalysts (type C, mode II) at A/F = 14.2. *Solid lines* Pd/Fe-10A2B. *Dotted lines* Pd/CeO_2-ZrO_2. Temperature ramp: 20 °C min^{-1}

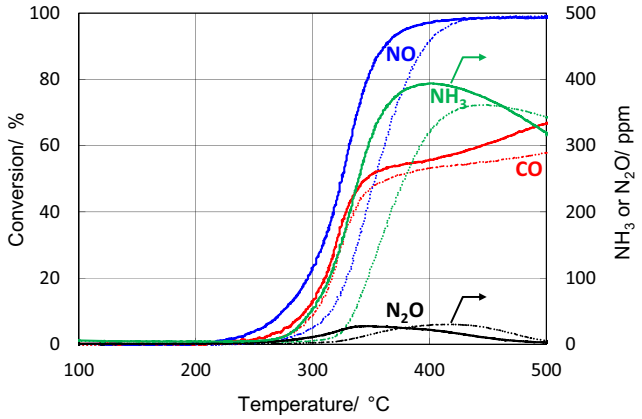

Fig. 10 Catalytic light-off curves of CO–NO–O_2–H_2O–N_2 and NH_3/N_2O formation over monolayer honeycomb catalysts (type C, mode III) at A/F = 14.2. *Solid lines* Pd/Fe-10A2B. *Dotted lines* Pd/CeO_2-ZrO_2. Temperature ramp: 20 °C min^{-1}

a promising catalyst support for the development of automotive catalysts with decreased Rh contents. The monolayer-coated catalyst containing Pd/Fe-10A2B demonstrated characteristic features under a fuel-rich atmosphere, in which CO–H_2O and subsequent NO–H_2 reactions significantly accelerated NO conversion.

Acknowledgments This study was supported by the 'Elements Science and Technology Project' of MEXT Japan as well as by the MEXT programme 'Elements Strategy Initiative to Form Core Research Centers'.

References

1. Heck, R.M., Farrauto, R.J., Gulati, S.T.: Catalytic air pollution control: Commercial technology. Wiley (1995)
2. Shelef, M., Graham, G.W.: Why rhodium in automotive three-way catalysts? Catal. Rev. Sci. Eng. **36**, 433–457 (1994)
3. Shelef, M.: Nitric oxide: surface reactions and removal from auto exhaust. Catal. Rev. Sci. Eng. **11**, 1–40 (1975)
4. Taylor, K.C.: Nitric oxide catalysis in automotive exhaust systems. Catal. Rev. Sci. Eng. **35**, 457–481 (1993)
5. Gandhi, H.S., Graham, G.W., McCabe, R.W.: Automotive exhaust catalysis. J. Catal. **216**, 433–442 (2003)
6. Tanaka, H., Taniguchi, M., Uenishi, M., Kajita, N., Tan, I., Nishihata, Y., Mizuki, J.I., Narita, K., Kimura, M., Kaneko, K.: Self-regenerating Rh- and Pt-based perovskite catalysts for automotive-emissions control. Angew. Chem. Int. Ed. **45**, 5998–6002 (2006)
7. Nishihata, Y., Mizuki, J., Akao, T., Tanaka, H., Uenishi, M., Kimura, M., Okamoto, T., Hamada, N.: Self-regeneration of a Pd-perovskite catalyst for automotive emissions control. Nature **418**, 164–167 (2002)
8. Tanaka, H., Uenishi, M., Taniguchi, M., Tan, I., Narita, K., Kimura, M., Kaneko, K., Nishihata, Y., Mizuki, J.I.: The intelligent catalyst having the self-regenerative function of Pd, Rh and Pt for automotive emissions control. Catal. Today **117**, 321–328 (2006)
9. Nagai, Y., Dohmae, K., Ikeda, Y., Takagi, N., Tanabe, T., Hara, N., Guilera, G., Pascarelli, S., Newton, M.A., Kuno, O., Jiang, H., Shinjoh, H., Matsumoto, S.I.: In situ redispersion of platinum autoexhaust catalysts: an on-line approach to increasing catalyst lifetimes. Angew. Chem. Int. Ed. **47**, 9303–9306 (2008)
10. Nagai, Y., Hirabayashi, T., Dohmae, K., Takagi, N., Minami, T., Shinjoh, H., Matsumoto, S.I.: Sintering inhibition mechanism of platinum supported on ceria-based oxide and Pt-oxide–support interaction. J. Catal. **242**, 103–109 (2006)
11. Tanabe, T., Morikawa, A., Hatanaka, M., Takahashi, N., Nagai, Y., Sato, A., Kuno, O., Suzuki, H., Shinjoh, H.: The interaction between supported Rh- and Nd_2O_3-enriched surface layer on ZrO_2 for Rh sintering suppression. Catal. Today **184**, 219–226 (2012)
12. Tanabe, T., Nagai, Y., Dohmae, K., Sobukawa, H., Shinjoh, H.: Sintering and redispersion behavior of Pt on Pt/MgO. J. Catal. **257**, 117–124 (2008)
13. Hatanaka, M., Takahashi, N., Tanabe, T., Nagai, Y., Dohmae, K., Aoki, Y., Yoshida, T., Shinjoh, H.: Ideal pt loading for a Pt/CeO_2-based catalyst stabilized by a Pt-O-Ce bond. Appl. Catal. B Environ. **99**, 336–342 (2010)
14. Newton, M.A.: Dynamic adsorbate/reaction induced structural change of supported metal nanoparticles: heterogeneous catalysis and beyond. Chem. Soc. Rev. **37**, 2644–2657 (2008)
15. Kwak, J.H., Hu, J., Mei, D., Yi, C.W., Kim, D.H., Peden, C.H.F., Allard, L.F., Szanyi, J.: Coordinatively unsaturated Al^{3+} centers as binding sites for active catalyst phases of platinum on γ-Al_2O_3. Science **325**, 1670–1673 (2009)
16. Hinokuma, S., Fujii, H., Okamoto, M., Ikeue, K., Machida, M.: Metallic Pd nanoparticles formed by Pd–O–Ce interaction: a reason for sintering-induced activation for CO oxidation. Chem. Mater. **22**, 6183–6190 (2010)
17. Machida, M., Murakami, K., Hinokuma, S., Uemura, K., Ikeue, K., Matsuda, M., Chai, M., Nakahara, Y., Sato, T.: $AlPO_4$ as a support capable of minimizing threshold loading of Rh in automotive catalysts. Chem. Mater. **21**, 1796–1798 (2009)
18. Chen, X., Cheng, Y., Seo, C.Y., Schwank, J.W., McCabe, R.W.: Aging, re-dispersion, and catalytic oxidation characteristics of model Pd/Al_2O_3 automotive three-way catalysts. Appl. Catal. B Environ. **163**, 499–509 (2015)
19. Zou, W., Gonzalez, R.D.: Thermal stability of silica supported palladium catalysts prepared by the sol–gel method. Appl. Catal. A Gen. **126**, 351–364 (1995)
20. Abbas-Ghaleb, R., Garbowski, E., Kaddouri, A., Gelin, P.: $Al_{18}B_4O_{33}$ aluminium borate: a new efficient support for palladium in the high temperature catalytic combustion of methane. Catal. Today **117**, 514–517 (2006)
21. Ikeue, K., Watanabe, K., Minekishi, T., Imamura, A., Sato, T., Nagao, Y., Nakahara, Y., Machida, M.: Fe-substituted $10Al_2O_3 \cdot 2B_2O_3$ as a multifunctional support for automotive Pd catalysts. Appl. Catal. B Environ. **146**, 50–56 (2014)
22. Ikeue, K., Hinokuma, S., Watanabe, K., Minekishi, T., Sato, T., Nakahara, Y., Machida, M.: Structure and catalytic properties of Pd/$10Al_2O_3 \cdot 2B_2O_3$. Effect of preparation routes and additives. Bull. Chem. Soc. Jpn. **85**, 468–474 (2012)
23. Béguin, B., Garbowski, E., Primet, M.: Stabilization of alumina by addition of lanthanum. Appl. Catal. **75**, 119–132 (1991)
24. Bettman, M., Chase, R.E., Otto, K., Weber, W.H.: Dispersion studies on the system La_2O_3 − γ-Al_2O_3. J. Catal. **117**, 447–454 (1989)
25. Schaper, H., Doesburg, E.B.M., Van Reijen, L.L.: The influence of lanthanum oxide on the thermal stability of gamma alumina catalyst supports. Appl. Catal. **7**, 211–220 (1983)
26. Johnson, M.F.L.: Surface area stability of aluminas. J. Catal. **123**, 245–259 (1990)
27. Oudet, F., Courtine, P., Vejux, A.: Thermal stabilization of transition alumina by structural coherence with $LnAlO_3$ (Ln = La, Pr, Nd). J. Catal. **114**, 112–120 (1988)
28. Schaper, H., Doesburg, E.B.M., De Korte, P.H.M., Van Reijen, L.L.: Thermal stabilization of high surface area alumina. Solid State Ionics **16**, 261–265 (1985)

29. Gandhi, H.S., Graham, G.W., McCabe, R.W.J.: Catalysts **216**, 433–442 (2003)
30. Taylor, K.C.: Catal. Rev. Sci. Eng. **35**, 457–481 (1993)
31. Yao, H.C., Yao, Y.F.Y.: Ceria in automotive exhaust catalysts: I. Oxygen storage. J. Catal. **86**, 254–265 (1984)
32. Fisher, G., Theis, J., Casarella, M., Mahan, S.: The role of ceria in automotive exhaust catalysis and obd ii catalyst monitoring. SAE Paper, 931034 (1993)
33. Ozawa, M., Kimura, M., Isogai, A.: The application of Ce–Zr oxide solid solution to oxygen storage promoters in automotive catalysts. J. Alloys Compd. **193**, 73–75 (1993)
34. Kašpar, J., Fornasiero, P., Graziani, M.: Use of CeO_2-based oxides in the three-way catalysis. Catal. Today **50**, 285–298 (1999)
35. Trovarelli, A.: In: Trovarelli, A. (ed.) Catalysis by ceria and related materials. Imperial College Press, London (2002)